Underwater Ultrasonic Wireless Power Transfer: A Battery-less Platform for the Internet of Underwater Things

Raffaele Guida, *Student Member, IEEE,* Emrecan Demirors, *Member, IEEE,* Neil Dave, and Tommaso Melodia, *Fellow, IEEE*

Abstract—The Internet of Underwater Things (IoUT) will enable new military, scientific, and commercial applications at sea. However, powering of electronic devices in deep water still remains one of the main challenges, since these systems are typically powered by traditional batteries. This article presents the design of the first batteryless underwater sensor node that can be wirelessly recharged through ultrasonic waves from longer distances than allowed by current technologies. First, the architecture of an underwater platform capable of extracting electrical energy from ultrasonic waves is introduced. We then illustrate how to interface this system with an underwater digital communication unit. We discuss the design of a prototype where the storage unit is realized with a batch of supercapacitors. We show through experiments that the harvested energy is sufficient to provide the sensor node with the power necessary to perform a sensing operation and power a modem for ultrasonic communications. In the article, we evaluate the system power transfer efficiency. Given the reduced attenuation of ultrasonic waves in water, we show that our approach can cover longer distances with less transmission power than alternative solutions. Last, we experimentally evaluate the overall operating efficiency of the system.

Index Terms—Internet of Things (IoT), Wireless Power Transfer (WPT), Ultrasonic Communications

1 Introduction

Underwater networking technologies have been a key enabler for many military, commercial, and scientific applications, including (i) tactical/coastal surveillance; (ii) control and monitoring systems for the oil and gas industry; (iii) climate change monitoring, pollution control and tracking; and (iv) commercial exploitation of the aquatic environment, among others [2], [3], [4]. We envision that the increasing number of applications will eventually lead to a vast deployment of underwater objects and enable the Internet of Underwater Things (IoUT) on a larger scale. The architecture of underwater objects (e.g., underwater wireless sensor network nodes (UWSNs) and autonomous underwater vehicles (AUVs)) is increasingly becoming more complex. These systems will encompass multiple sensors, wireless communication systems, actuators, and rotors or propulsors which will inevitably increase the total power requirement. Often, an underwater sensor node requires about 30 W of power for non-propulsion related functions (communication, processing, and sensing), on top of which another 15–110 W are needed if the device includes propellers or other mechanical components [5]. Supplying these levels of power to underwater sensor nodes and vehicles over long periods of time still remains an open problem.

Batteries are the most common solution to power underwater devices. However, a remotely operated vehicle with the support of a vessel is generally required to recharge or replace these batteries. These operations are very expensive and non-scalable [6]. Moreover, given the inaccessibility and dynamic movement of the nodes, the charging operations are often difficult and inefficient, as precise alignment between the transmitter and the receiver is often required [7]. For example, some recharging solutions for AUVs are limited in their usage, as they call for wet mate connectors that, in addition, are prone to failure. Energy harvesting, successfully applied to traditional wireless sensor networks (WSNs), is challenging in the underwater environment because natural sources, such as solar or wind energy, are unavailable or inefficient.

In recent years, researchers have investigated wireless power transfer (WPT) technologies to remotely power underwater sensors. The most widely investigated techniques are based on electromagnetic (EM) propagation in the near field region, namely inductive and magnetic coupling (see Table 1). Even though the majority of prototypes have shown efficiency values above 65%, the maximum operation distances are limited to few centimeters with inductive coupling, and one order of magnitude higher with magnetic coupling. Additionally, very precise alignment between the transmitting and the receiving coil is typically necessary.

Because of their lower attenuation in aqueous media, acoustic waves are a promising alternative to EM induction for realizing WPT in underwater systems. Acoustic propagation in water can cover longer distances while losing less power when compared to EM-based methods. This means that ultrasonic WPT technologies for remote recharging operations are feasible because the charger and the nodes can be placed further apart. In this article, we present the architecture of a platform equipped with ultrasonic connectivity for IoUT that can be remotely charged via acoustic waves, eliminating the need for large batteries. Ultrasonic communications have been extensively investigated in UWSN applications, but the literature on ultrasonic WPT in underwater environments is more sparse. In this article, we demonstrate for the first time a batteryless underwater

• *R. Guida, E. Demirors, and T. Melodia are with the Institute for the Wireless Internet of Things, Northeastern University, Boston, MA, 02115 USA (e-mail: {guida.r, e.demirors, melodia}@northeastern.edu).*
• *N. Dave is with Bionet Sonar, Burlington, MA 01803 USA (e-mail: neil@bionetsonar.com).*
• *A preliminary, shorter version of this article [1] appeared in the Proceedings of IEEE Underwater Communications Conference (UComms) 2018.*
• *This work was supported by the National Science Foundation under Grant CNS-1618727 and Grant CNS-1763709.*

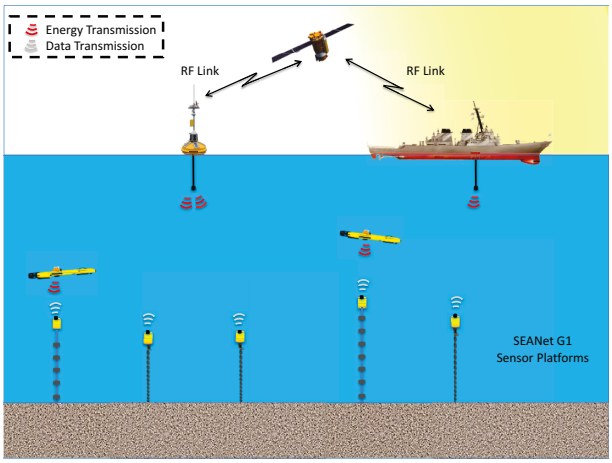

Fig. 1. An application scenario enabled by the battery-less IoUT platforms.

sensor node that can be powered through ultrasonic energy transfer.

Novelty

We propose a system that is novel for the following aspects. Our system uses ultrasonic waves as a medium to carry energy to a remote underwater modem, enabling a battery-less and wirelessly powered platform for the IoUT. The use of supercapacitors, replacing traditional or rechargeable batteries, makes the system lighter, easier and faster to recharge. All the components of the underwater modem are powered from the same energy storage component, therefore, we specifically design a powering unit to overcome the challenges arising from interfacing the energy management unit with the communication unit. Leveraging ultrasonic WPT, the system energy can be restored with about 1 W of power at a distance of $1\mathrm{m}$ in less than $5\mathrm{min}$. We also conduct a study on the acoustic underwater wireless link showing that longer distances than state-of-art technologies can be covered. We design a system that uses only one transducer both for charging and communication, which saves space, weight, and cost. This design choice, on the other hand, requires a proper switching mechanism. We demonstrate a practical implementation of an ultrasonically rechargeable UWSN node, reporting key design aspects to improve the efficiency of the system (*e.g.* matching network and the use of different supercapacitors configurations).

The reminder of this article is organized as follows. Section 2 provides background material and an overview of powering techniques in underwater networks. In Section 3 the proposed system architecture and its operating principle are presented. In Section 4 we describe the underlying physical principles of wave and fields attenuation in the cases of electromagnetic (EM) waves, magnetic induction (MI), and ultrasound (US) in fresh and sea water. In Section 5 we describe the design and the evaluation metrics of our WPT system enabled with ultrasonic communication capabilities. The system prototype and the experimental results are illustrated in Section 6 and section 7, respectively. We conclude the article in Section 8.

2 Overview of Powering Techniques Underwater

Traditionally, underwater sensor nodes and autonomous vehicles are powered by batteries or rechargeable batteries. However, battery replacement in underwater environments is a complex and expensive operation. For example, a vessel may be required to support the operation, or automatic retrieval and insertion mechanisms may be needed. Moreover, a wet connection from the battery to the underwater device needs to be established [8]. Even though this solution allows to have a new power supply with a transfer efficiency of virtually 100% and without waiting for a recharging operation time, batteries are an environmental hazard and their use is limited by governments. Therefore, the battery pack has to be sealed against corrosive waters and a mechanism for venting evolved gasses is also necessary [8]. Batteries can be problematic also in terms of lifetime. Underwater systems require higher levels of power to operate when compared to their ground counterparts, thus the battery duration can be drastically shorter unless larger or multiple batteries are used. For instance, underwater sensor nodes enabled with acoustic and optical communication interfaces reported in [9] were able to operate for only two weeks. Inter-node distance and communication frequency are other factors that severely affect the battery lifetime. Specifically, the battery life decreases exponentially when increasing the communication link distance or the frequency [10].

Seawater batteries are a special category of batteries that use alternative renewable energy sources, such as the oxygen present in seawater, to produce electricity. When the water that serves as the electrolyte flows through the cathode of the cell, it releases oxygen while the force of the flow removes the deposits from the electrodes of the battery. However, seawater batteries life duration and performance are not easily predictable because they depend on the hydrodynamic conditions and the specific location where they are deployed. For more details about seawater batteries, the reader can refer to [10].

2.1 Underwater energy harvesting

Harvesting energy from the environment surrounding the UWSNs is one of the two alternative approaches to batteries and a solution to provide the electrical energy to refill rechargeable storage components (e.g., capacitors, supercapacitors, or secondary cells) underwater. The best energy sources in rivers, seas, and oceans are (i) kinetic energy in the form of underwater currents, tides, waves and vibrations, (ii) electrochemical activity of bacteria, (iii) solar energy in case of more superficial applications [10], [11], [12].

Piezoelectric materials are used to extract energy from kinetic energy sources. These types of underwater harvesters can reach powers from the order of milliwatts to few watts. An example of energy harvesting from vibrations is reported in [13]. The article reports on a piezoelectric composite beam measuring $95\ \mathrm{mm} \times 35\ \mathrm{mm} \times 0.8\ \mathrm{mm}$. Experimental results show that by submerging the structure at different lengths, values of power of few microwatts can be extracted. The Energy Harvesting Eel (Eel) [14] is a commonly referenced application that exploits the piezoelectric effect to harvest energy from flows present in oceans and rivers. The Eel consists of long strips of piezoelectric polymers that move in an oscillatory motion when the harvester is immersed in water. Because of this undulating motion, a strain is produced on the polymers that generates a low-frequency AC voltage. After AC-to-DC conversion, the rectified voltage is used to charge an electric storage.

Turbines and rotors are mainly adopted to convert hydropower, power of falling or moving water, into electricity. The electromagnetic induction is the physical principle at

This article has been accepted for publication in a future issue of this journal, but has not been fully edited. Content may change prior to final publication. Citation information: DOI 10.1109/TMC.2020.3029679, IEEE Transactions on Mobile Computing

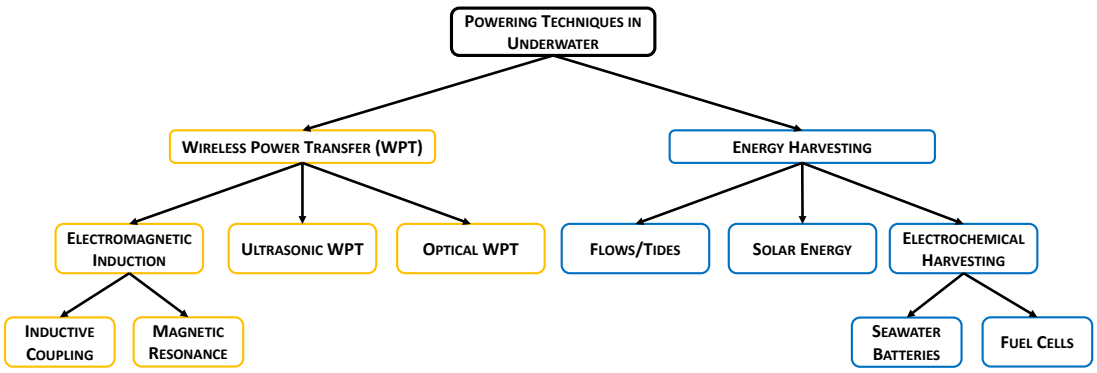

Fig. 2. Schematization of the powering techniques underwater.

the base of these converters [15] that typically include a mechanism including a closed circuit and a magnet. According to the Faraday-Neumann law, when the circuit moves relatively to the magnet, an electromotive force is induced into the circuit. Off-the-shelf hydro-based energy harvesters can produce levels of power of the order of few kilowatts, however they would add complexity to the underwater sensor nodes and make them bulkier.

Triboelectric nanogenerators (TENGs) can also be used together with a rotor to transform mechanical energy of moving water to electrical energy. TENGs can also reduce the dimensions of the harvester. For example, a recent study [16] proposed a rotary triboelectric nanogenerator whose dimensions are of the order of a few tens of square centimeters, and with the maximum power flow of $44\ \mathrm{L/min}$ is capable of producing $6.1\ \mathrm{W/m^2}$ of power. In practical terms, it means that the device can power about 50 series-connected light emitting diodes, and fully charge a $0.1\ \mu\mathrm{F}$, $15.2\ \mathrm{V}$ capacitor in $65\ \mathrm{s}$. Another TENG, presented by Su et al. in [17], was designed to simultaneously harvest two types of energy provided by water waves, namely the impact mechanical energy and the electrostatic energy due to the interface between water and the solid surface of the TENG itself. Therefore, the system has an interfacial electrification TENG to collect the electrostatic energy and an impact TENG. Experimental results show that the two TENGs can generate less than $10\ \mu\mathrm{A}$ of current and a few tens of microwatts in total. However, the storage charging performance of these systems are still ineffective because more power is needed to collect the necessary amount of energy to activate an underwater modem as we will show in our system design and experimental results. Moreover, as observed before, the energy produced by these types of harvesters is not always predictable, since the source (water flows) can be time-variant.

Microbial fuel cells (MFCs) is the technology used to exploit the metabolic activities of water micro-organisms as a renewable energy source and convert it to electrical energy to power IoUT systems [15]. Similar to batteries, MFCs have two electrodes, an anode and a cathode. The first one is buried in sediment where there is no oxygen and the cathode submerged in water above the sediment. The anaerobic micro-organisms in the sediment produce electrons by degrading organic matter (oxidation process). These electrons are transferred to the anode and flow towards the cathode generating a current that passes through the load attached to the MFC [18], [19]. As of today, the majority of the MFCs are reported to provide only few microwatts of power [19], [20]. A previous work by Donovan et al. [21] reports on a successful implementation of a power management system (PMS) that allows a MFC to activate a wireless sensor requiring $2.5\ \mathrm{W}$ of power. The energy derived from the microbial fuel cell is stored in capacitors and then periodically conveyed to the sensor in bursts so that the capacitors have enough time to be replenished between two transmissions. Since the power provided by the bacterial oxidation process is low, it takes several hours to completely charge the capacitors and approximately $27\ \mathrm{min}$ between two transmissions, which constitutes the major drawback of this system.

We omit a detailed discussion on solar energy scavengers since they are employed in more superficial applications and in AUVs that can operate closer to the surface and harvest solar energy.

2.2 Underwater wireless power transfer (WPT)

Another major approach to deliver energy to submerged sensing nodes and other electronic devices is wireless power transfer (WPT) as shown in the diagram in Figure 2. WPT consists in sending power from a remote transmitting source to a destination (receiving device) wirelessly by means of a wave propagation phenomena. Different physical principles can be exploited to implement a WPT system. As reported in Figure 2, these principles include electromagentic-based induction (such as near-field inductive coupling and mid-field magnetic resonance effect), ultrasonic waves, and propagation of light.

Electromagnetic couplers can be realized either with coils or with spirals. Multiple studies compare coil-based to spiral-based inductive coupling. Generally, WPT by means of spiral inductors provides better performance in water. This is confirmed by both simulation and experimental results [6], [22]. The work in [6] reports experimental efficiency values higher than 60% and 75% for coil and spiral-based inductors, respectively, at a distance of $5\mathrm{cm}$. Similarly, simulation results of inductive coupling in seawater show an approximately constant efficiency in the range of 65–80% in the over-coupled region up to $8\ \mathrm{cm}$ for a coil, and up to $13\ \mathrm{cm}$ for a spiral [22]. A white paper released by WiTricity [23] reports the simulation results of a WPT method based on magnetic coupling showing an efficiency of about 80%. A practical implementation of the same system reaches efficiency values of 15% less than the simulated results.

In [24] a study is conducted on radio frequency-based communications and inductive energy transfer in underwater environments. Experimental results demonstrate the feasibility of underwater communications at $2.4\ \mathrm{GHz}$ up to

This article has been accepted for publication in a future issue of this journal, but has not been fully edited. Content may change prior to final publication. Citation information: DOI 10.1109/TMC.2020.3029679, IEEE Transactions on Mobile Computing

TABLE 1
Comparison between WPT techniques underwater.

Ref.	Type	Distance [cm]	Tx/Rx power	Eff. (%)
[24]	Inductive coupling	4 7	Tx=−25 dBm Tx=−3 dBm	50
[25]	Inductive coupling	-	Rx=10 kW	91
[6]	Inductive coupling	5	-	60–75
[22]	Inductive coupling (simul.)	8–13	-	65–80
[26]	Eddy current propagation	10 5	- -	60 50
[27]	Magnetic coupling	0.2	-	90
[23]	Magnetic coupling	15 (simul.) 26 (exper.)	Rx=3 kW -	~80 ~65
[28]	Ultrasonic WPT	100	Rx=~mW	-

The values reported in the table are for experimental results if not differently indicated.

4 cm with −25 dBm of transferred power and up to 7 cm with −3 dBm. The wireless power transfer efficiency of the system is approximately 50%.

Ultrasonic WPT was demonstrated in [28] where power values on the order of milliwatts were measured over a distance of 1 m. The feasibility of a system able to wirelessly power underwater sensors from an acoustic source was proved through an analytical model in [29]. However, to the best of our knowledge, no other study has further investigated the possibility of using ultrasonic waves for underwater WPT through a practical implementation.

Efficient energy storage and power management are essential support services for underwater mobile nodes and networks. WPT is a promising technology to recharge AUVs and, in general, underwater mobile devices. Long distance WPT approaches allow mobility of drones and nodes in a network, and easier charging operations by:

1) Avoiding cables that are normally required to power or recharge underwater devices making it easier to power drones out at sea. For instance, with current recharging methods, the nodes need to dock to a surface ship or land to be recharged [30]. This limits the autonomy of the nodes and interrupts or limits the operations in a network. Another issue with either underwater or surface docking stations is the difficulty of the nodes to plug themselves into the charging device.
2) Removing human-in-the-loop in the recharging process. Currently, underwater drones must return to their base to be manually connected to a charging station or to replace their batteries. Conversely, WPT allows to remotely deploy wireless charging stations in the areas where UWSNs and AUVs operate, removing the human element from the charging phase.
3) Charging multiple nodes simultaneously from the sar wireless power source. Restoring the energy in the nod of an underwater network by means of energy harve ing, batteries or cables is a non-scalable approach, as ea node requires its own harvester or the devices can recharged only one at a time. Instead, it has already be demonstrated that an ultrasonic WPT system can pow multiple nodes at the same time [29].
4) When compared to energy harvesting, WPT allows reuse hardware components reducing size, complex and cost of the platform. For example, a node c use the same antenna or ultrasonic transducer (as v demonstrate in the system proposed in this article) bc for charging and data communication. Devices that u energy harvesting, instead, require an *ad-hoc* harvesti structure that in many cases limits the mobility of the node (see the Eel as an example [14]).

3 System Overview

In this section we briefly describe the architecture and operating principle of a battery-less platform for the IoUT powered by ultrasonic WPT with ultrasonic telemetry. Figure 1 shows an application scenario enabled by the battery-less IoUT platforms. A set of battery-less IoUT platforms equipped with different sensors is deployed and anchored to the bottom of the ocean/sea. These platforms are wirelessly powered through acoustic waves either by surface objects, such as ships or buoys, or submerged objects, such as remotely operated vehicles (ROVs) or unmanned underwater vehicles (UUVs), to perform sensing operations and transmit their sensed data back to the charging objects. The data collected by the charging objects can eventually be globally accessible through a radiofrequency (RF) link.

The general architecture of the proposed batteryless IoUT platform is shown in Figure 3. The system includes three main modules, namely a SEANet node, which serves as an underwater communication and sensing platform [31], an *energy management unit* to receive, convert and store the energy, and a *powering unit* to power the platform components. The core building block of the communication unit is a Teensy board that is a microcontroller development system that receives and processes the data from a sensor. It is also capable of generating signals containing the processed data based on the Zero-Padded Orthogonal Frequency-Division-Multiplexing (ZP-OFDM) communication scheme.

The operation of the system can be divided into two phases. Initially, the energy buffer is completely or partially depleted. Therefore a remote charger must send energy to the system via ultrasonic waves so the node can be recharged. After enough energy has been stored, the system enters the second phase, in which the energy is used to power the SEANet node for sensing and data transmission operations.

4 Absorption of Electromagnetic and Ultrasonic Waves Underwater

In this section, we present models of propagation of electromagnetic (EM) waves in the *far-field* region, magnetic inductance in the *near-field* region, and ultrasonic waves.

The analytical models included in this Section provide a mathematical formulation of the principles of the most common approaches to WPT underwater. This brief discussion, firstly aims to clarify the propagation phenomena that are at the basis of different WPT techniques underwater. Since

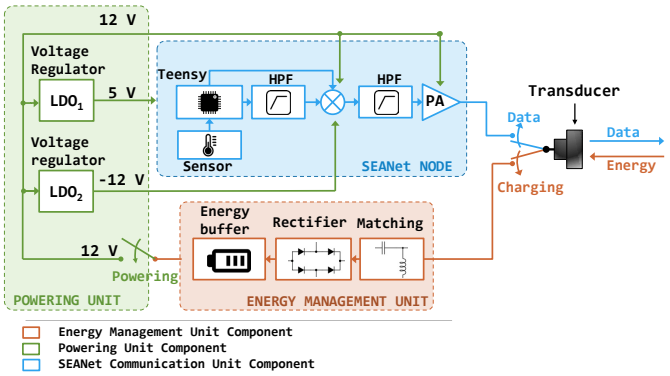

Fig. 3. Block diagram of the ultrasonically rechargeable IoT platform.

This article has been accepted for publication in a future issue of this journal, but has not been fully edited. Content may change prior to final publication. Citation information: DOI 10.1109/TMC.2020.3029679, IEEE Transactions on Mobile Computing

the propagation of waves is affected by water conductivity, salinity, etc. it is essential to understand and compare the propagation of electromagnetic radiation, magnetic induction, and ultrasonic waves both in fresh and sea waters. Second, the study provides a quantitative analysis of the transmission losses for different types of waves (electromagnetic and mechanical); third it is key to understand to which extent the use of ultrasonic waves to carry power and data - instead of other wireless technologies - can be more efficient over long distances and on a resource-limited (and even battery-less) device as the IoUT platform that we propose. For example, as showed in Figure 7, the attenuation of EM waves in sea water, after few centimeters from the transmitter, is of at least two orders of magnitude higher than ultrasonic waves, which means that the received power would be of at least two orders of magnitude smaller (in the order of nano-watts for 1W of transmitted power). The direct consequences of this inefficiency are longer charging times (that affect the data rate as we will see in Section 6), transmission powers of two orders of magnitude higher required to the IoUT platform to transmit data and relative larger energy storage; or alternatively more complex, sensitive and expensive transceiver electronics. We aim to design a battery-less device powered with supercapacitors that are easier and faster to recharge than batteries. In such system, the recharges can be frequent, therefore we need an efficient way to transfer the energy to the node to charge it quickly. Furthermore, the charging duration affects the end-to-end data rate of the system. Thus, the analytical models in Section 3 allow us, not only to select the most efficient methodology among other valid alternative technologies, but they also enable us to: (i) have a reference model to design our system (ii) verify that our setup, specifically the wireless ultrasonic link, behaves according to the theory. For example, to account for the power transmission loss, we defined the power transfer efficiency (Section 5) that allowed us to design the link and the energy management unit of the platform, and to measure its performance.

4.1 Models for EM Propagation in Water

The intrinsic properties of seawater strongly impact the propagation of electromagnetic (EM) waves travelling through them. For simplicity, let us consider a linearly polarized EM wave propagating in a medium along the z direction. The solutions to the Maxwell's equations, namely the strength of the electric field E_x and the strength of the magnetic field H_y, respectively, are [32]

$$E_x = E_0 \cdot e^{(j\omega t - \gamma z)} \tag{1}$$

$$H_y = H_0 \cdot e^{(j\omega t - \gamma z)}, \tag{2}$$

where E_0 and H_0 are the strengths of the electric and of the magnetic field at the transmitting source, respectively. The propagation constant γ is a complex quantity that depends on the permittivity $\epsilon(\omega)$, the magnetic permeability μ, the conductivity σ, and the angular frequency ω. γ can be written as [32]

$$\gamma = \alpha - j\beta = j\omega\sqrt{\epsilon\mu - j\frac{\sigma\mu}{\omega}}, \tag{3}$$

where α is the attenuation factor (or *attenuation coefficient*) and β the phase factor.

In Table 2 we report the main symbols and constants used in the models described in this section.

TABLE 2
Main symbols and constants

Symbol	Name	Value or equation
j	Imaginary unit	$\sqrt{-1}$
f	Frequency	-
ω	Angular frequency	$2\pi f$
ϵ_0	Permittivity of vacuum	$8.85 \cdot 10^{-}12$ [F/m]
ϵ_s	Real relative permittivity of water at low frequencies	81, (4)
ϵ_∞	Real relative permittivity of water at high frequencies	4.5
$\epsilon_r(\omega)$	Relative permittivity of the medium	(4)
$\epsilon(\omega)$	Permittivity of medium	$\epsilon_0\epsilon_r(\omega) = \epsilon'(\omega) - j\epsilon''(\omega)$
μ_0	Magnetic permeability of vacuum	$4\pi \cdot 10^{-}7$ [H/m]
μ_r	Relative magnetic permeability of water	1
μ	Magnetic permeability	$\mu_0\mu_r$
γ	Propagation constant	(3)
σ	Electrical conductivity	-
σ_{fw}	Electrical conductivity of fresh water	$0.005 - 0.01$ [S/m]
σ_{sw}	Electrical conductivity of sea water	4 [S/m]
f_{ref}	Relaxation frequency	17.4 [GHz]
N, N_{tx}, N_{rx}	Number of turns of coils (tx transmitting, rx receiving)	-
T	Temperature	in °C
S	Salinity of water	in parts per thousand (ppt)

Several models have been proposed in literature to describe the attenuation of electromagnetic fields both in fresh and sea waters. Following we compare some of these models for EM propagation and magnetic induction in water.

4.1.1 Model 1: EM propagation in fresh water [33]

As Jiang et al. [33] indicate, the main source of attenuation of electromagnetic waves in water is due to the high conductivity (σ) of the medium. Moreover, σ increases with salinity, in fact for fresh water σ varies between 0.005 [S/m] and 0.01[S/m], but in sea water $\sigma = 4$[S/m] [34]. The attenuation in sea water is higher, as we show in Figure 4. The model in [33] uses the Debye equation to describe the frequency dependent dielectric permittivity of fresh water, which is:

$$\epsilon_r(f) = \epsilon_\infty + \frac{\epsilon_s - \epsilon_\infty}{j\frac{f}{f_{ref}}} - \frac{j\sigma}{2\pi f\epsilon_0}. \tag{4}$$

The attenuation α is the real part of γ expressed as

$$\alpha(f) = \mathrm{Re}(\gamma) = \mathrm{Re}\left(\sqrt{j\omega\mu(\sigma + j\omega\epsilon_r(f))}\right) \tag{5}$$

and the propagation loss in dB due to the attenuation is

$$A_{dB} = 10\log_{10}\left(e^{2\alpha d}\right), \tag{6}$$

where d is the distance of propagation in meters. In order to compare this model with other solutions, we consider only the attenuation of a wave that has a normal incidence on the surface of the water and we omit the losses for oblique incidence.

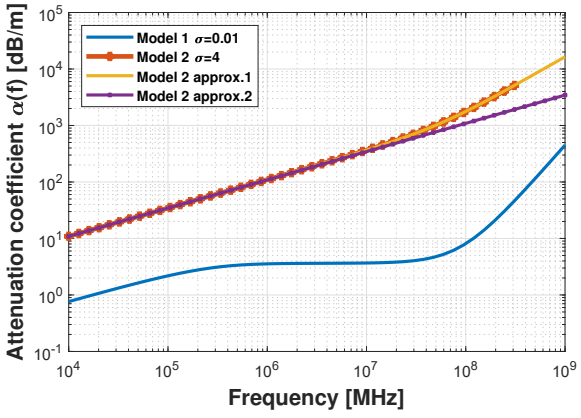

Fig. 4. Attenuation coefficients for different models of EM wave propagation in fresh water ($\sigma = 0.01$) and sea water ($\sigma = 4$).

This article has been accepted for publication in a future issue of this journal, but has not been fully edited. Content may change prior to final publication. Citation information: DOI 10.1109/TMC.2020.3029679, IEEE Transactions on Mobile Computing

4.1.2 Model 2: EM propagation in sea water [34]

Similarly to Model 1, Karagianni et al. [34] propose an analytical model for EM wave propagation in sea water. They express the propagation constant γ as in (3) and consider fixed values for $\epsilon = 81$ and $\sigma = 4$. Thus, the attenuation in dB is

$$A_{dB} = 10 \log_{10} \left(e^{2\alpha d}\right) \approx 8.7 \alpha d. \tag{7}$$

The exact curve for the (7) is plotted in Figure 4.

4.2 Models for Near-field Magnetic Induction in Water

The formulations presented in the previous subsections are good models for electromagnetic waves propagation in water in the *far-field* region. However, the most common methods for WPT are based on inductive coupling, that characterizes the propagation in proximity of the radiating element, where the *far-field* approximation is no longer valid. The description of the fields becomes more complex and more accurate models are needed. A magnetic induction (MI)-based system consists of a transmitter coil that generates and modulates a magnetic field that couples with a receiving coil located at a distance r in the *near-field* region. The geometrical parameters, including dimensions and number of turns, influence the propagation of the field.

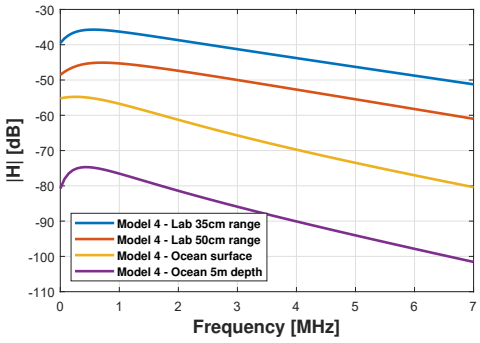

Fig. 5. Magnitude of the frequency response of the models for MI.

4.2.1 Model 3: MI in water [35]

The path loss of the model in [35] is calculated taking into account the geometrical and electrical parameters of the transmitting and receiving coil. The path loss (in dB) defined in this model is

$$PL_{MI} = -10 \log_{10} \frac{R_L \omega^2 M^2}{R_{tx} \left(R_L + R_{rx}\right)^2 + R_{tx} \left(X_L + \omega L_{rx}\right)^2}, \tag{8}$$

where R_L and X_L are the resistance and reactance of the load, respectively, M is the mutual inductance, L the self-inductance, and R the coil resistance. The (8) does not account for the attenuation due to the Eddy currents generated in sea water by the AC magnetic field. This additional loss can be taken into account with the (7). The total path loss in seawater is

$$PL_{sw} = PL_{MI} + 8.7 \alpha r, \tag{9}$$

where $\alpha = \sqrt{\pi f \mu \sigma}$ (from [35]).

4.2.2 Model 4: 7-parameter model for MI in water [36]

A 7-parameter model is presented in [36] to describe the magnetic induction in water (both fresh and sea water). The frequency-dependent transfer function $H(f)$ (in dB) of the channel (water) is

$$|H| = \frac{p_1 f^2 + p_2 f + p_3}{q_1 f^2 + q_2 + q_3} \cdot e^{-\alpha_3 f}. \tag{10}$$

The seven parameters p_i, q_i and α_3 were found experimentally and are listed in [36]. We will report the curves using the same parameters.

4.3 Models for Acoustic Propagation in Water

The behavior of ultrasonic waves in a fluid can be described by the pressure variation inside the material, because they propagate as mechanical waves. Let us consider a volume V of fluid of mass m, density $\rho = m/V$ and compressibility β. The wave equation for an ultrasonic wave propagating along the axis x a can be written as

$$\frac{\partial^2 \eta}{\partial x^2} = (\beta \cdot \rho) \frac{\partial^2 \eta}{\partial t^2}, \tag{11}$$

where η is the displacement along x. The pressure wave of an ultrasonic beam propagating through a medium is

$$p(x) = p_0 e^{-\alpha x} e^{j(\omega t - kx)}, \tag{12}$$

where k is the wave number. The (12) is a solution to the (11) since the pressure variation Δp is function of the displacement

$$\Delta p = -\frac{1}{\beta} \cdot \frac{\partial^2 \eta}{\partial t^2}. \tag{13}$$

Moreover, α is the attenuation factor that, for frequencies in the order of MHz, is $\alpha = \alpha_0 \cdot f^b$, where α_0 is the amplitude attenuation coefficient measured in [dB/cm/MHz]. Three major phenomena cause the attenuation of ultrasonic waves in sea water, namely the viscous absorption that is the contribution of pure water (significant at frequencies above 100 kHz), the chemical relaxation effects due to boric acid for low frequencies (up to a few kHz), and magnesium sulphate for frequencies up to 100 kHz [4], [37].

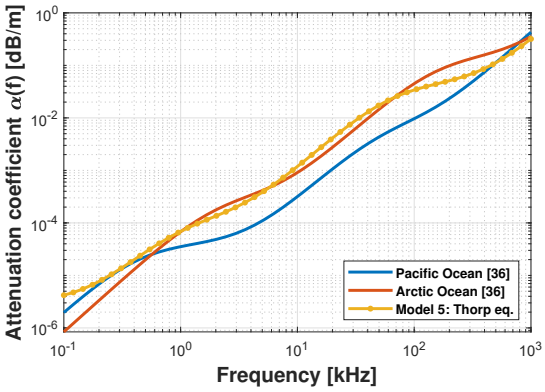

Fig. 6. Attenuation coefficients for different models of ultrasonic wave propagation in sea water.

This article has been accepted for publication in a future issue of this journal, but has not been fully edited. Content may change prior to final publication. Citation information: DOI 10.1109/TMC.2020.3029679, IEEE Transactions on Mobile Computing

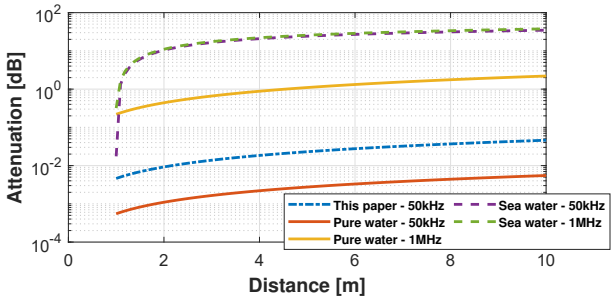

Fig. 7. Comparison of the attenuation (in dB) of ultrasonic waves in fresh water and sea water for varying distances and different frequencies.

4.3.1 Model 5: Thorp's formula for ultrasonic absorption in sea water

The absorption coefficient of acoustic waves underwater can be expressed using the Thorp's formula which is valid for frequencies above a few hundred Hz [4]. This formula defines $\alpha(f)$ in [dB/m] as a function of the frequency f in [kHz]

$$\alpha(f) = (0.11\frac{f^2}{f^2+1} + 44\frac{f^2}{f^2+4100} + 2.75\cdot 10^{-4} f^2 + \\ +0.003)\cdot 10^{-3}. \quad (14)$$

In this case, the transmission loss $A_{tot,dB}$ (that is $TL(d,f)$ expressed in dB) is a function of the frequency f in [kHz] and the distance d in [m] and is given by

$$A_{tot,dB} = 10\log(TL(d,f)) = k\cdot\log(d) + d\cdot A_D(f) + A, \quad (15)$$

where k is the spherical spreading factor, A (in dB) is the *anomaly factor* and it accounts for other effects such as multipath, refraction, diffraction and scattering [4]. $A_D(f)$ in [dB/m] is a depth-dependent factor and is equal to

$$A_D(f) = \alpha(f)(1 - 1.93\cdot 10^{-5}\cdot D), \quad (16)$$

where D is the depth in [m]. The (15) shows that the transmission path loss is mainly caused by two phenomena, namely the geometric spreading $k\cdot 10\log(d)$ and the attenuation $d\cdot A_D(f)$. We neglect the term A and choose $k = 1.5$ to plot the path loss in Figure 7, and $k = 0$ for Figure 8 and Figure 9 where we only consider the water absorption and not the geometric spreading. We also note that the term $10\log(d)$ is zero for distances $d < 1$ m.

The path loss of EM waves, MI and ultrasounds (US) are compared via numerical evaluations of Model 2, Model 3, and Model 5, respectively. The results are shown in Figure 7, Figure 8 and Figure 9. The transmission loss $10\log(TL(d,f))$ of ultrasonic waves for two frequencies (50kHz and 1MHz) is illustrated in Figure 7. The attenuation increases with the frequency over 10 m from about 0.01 dB to 30 dB. In all three cases (EM, MI, and US) the path loss increases with the distance, however electromagnetic propagation shows the worst results (Figure 8). For example, at 500 MHz, the transmission loss is 5000 dB at 5 m only. MI shows good results when compared with ultrasounds but only for the first 20 m of range as showcased in Figure 9. However, the results are valid for a magnetic inductor with coils of 2 m diameter which makes the system large and impractical.

5 System Architecture and Design

SEANet Communication Unit

A detailed description of the design of SEANet communication and sensing platform is reported in [31]. We briefly report the most important design requirements. The SEANet node can perform sensing and communication operations in 1.2 s broken down into 5 ms for powering-up, 800 ms for sensing and processing data from its temperature sensor, and 310 ms for transmission operations that can send one ZP-OFDM packet including eight ZP-OFDM symbols carrying 6144 bits of data. The ZP-OFDM scheme occupies a bandwidth of 11.025kHz at a center frequency of 22.050kHz. A high pass filter (HPF) connects the Teensy with a mixer and removes the DC offset from the waveforms. The mixer multiplies the waveforms with a signal of 27.950 kHz shifting them and producing waveforms centered at 50 kHz (22.050 + 27.950 kHz). The 50 kHz centered signals are high-pass filtered again and amplified (to increase the transmission power) before being transmitted over the wireless link by means of an ultrasonic transducer. To perform these operations of sensing and data transmission, the board requires a voltage of 12 V and 140 mA of current. Hence, the required power amounts to 1.68 W consuming 2.02 J of energy. However, not all components of the communication unit require the same supply voltage. Specifically, the Teensy is powered with 5 V, the mixer needs two "supply rails" (±12 V) and the power amplifier can only work with 12 V positive.

Energy Management and Powering Units

The energy management unit includes a traditional diode full wave rectifier connected to the transducer through a matching network. The matching between the transducer and the rectifier minimizes the impedance mismatch between the two components to maximize the unit's received power and consequently the wireless power efficiency (WPE), or power transfer efficiency (PTE). From the sinusoidal waveform, the rectifier extracts a constant voltage that is used to refill the energy storage, which needs a DC signal to be recharged. Two low drop out (LDOs) regulators provide different components with their required operative supply voltages. The system encompasses two MOSFET/ADC-based switches that connect the transducer to the energy management unit, and allow to power the data communication unit and activate the transmission once enough energy has been stored.

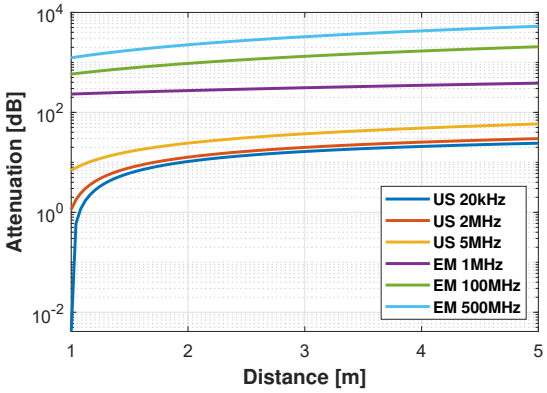

Fig. 8. Comparison of the attenuation (in dB) of ultrasonic waves (Model 5) and EM waves in the far-field region (Model 2) in sea water for varying distances and different frequencies.

This article has been accepted for publication in a future issue of this journal, but has not been fully edited. Content may change prior to final publication. Citation information: DOI 10.1109/TMC.2020.3029679, IEEE Transactions on Mobile Computing

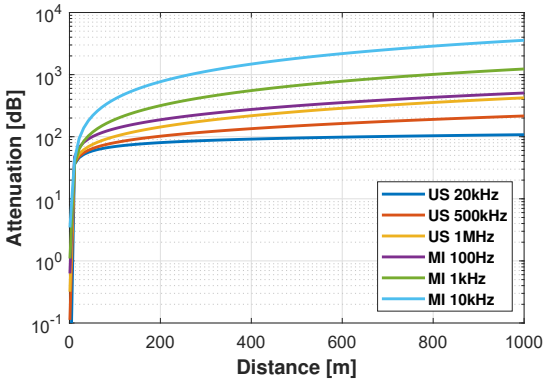

Fig. 9. Comparison of the attenuation (in dB) of ultrasonic waves (Model 5) and MI in the near-field region (Model 4) in sea water for varying distances and different frequencies.

Design Challenges

The design challenges relative to the energy management module are due to the received low power levels caused by the attenuation in water and conversion losses of the transmitting and receiving transducer. Furthermore, it is difficult to design an energy storage component that is small enough to be quickly recharged and that, at the same time can power the communication unit, for the following reasons: (i) the charging voltage across the supercapacitor has an asymptotic behavior in time when approaching full capacity; (ii) the maximum voltage rating of the storage component is typically lower than the voltage requirements of the communication circuit to which it has to provide its power; (iii) the internal equivalent series resistance (ESR) can be too large to provide the current needed by the load; (iv) as seen above, different parts of SEANet have different power and voltage needs.

Component design

From the SEANet energy requirements, the capacity needed to store the minimum amount of energy to activate the communication module can be calculated. The SEANet system needs 25 mF to be powered-up, and to sense and transmit one packet of data. It can be challenging or time consuming to charge a single capacitive element up to 12 V. Therefore, we use a bank of supercapacitors that are connected in parallel during the charging phase and in a different configuration during the powering phase so that the voltage across the equivalent capacitor configuration meets the load power requirements. In this way it is easier and faster to charge the whole set of supercapacitors and, after changing configuration, 12 V voltage can be provided to the SEANet components. Switching between the two phases is realized with a MOSFET and an ADC circuit. Different components of the communication circuit have different power requirements. Therefore, we include two low drop out (LDOs) regulators to adjust the storage supplied voltage and match the values required by the communication unit (Figure 3).

Evaluation metrics

The system performance was evaluated with the following metrics. The *charging efficiency*, defined as the ratio between the energy accumulated into the super-capacitors bank (E_s) and the total energy needed to charge it (E_{tx}), can be expressed as

$$\eta_c = \frac{E_s}{E_{tx}} \times 100. \tag{17}$$

The *effective data rate* η_d is defined in (18) and accounts for the total amount of data d_m (in $bits$) that can be sent with the harvested energy with respect to the time (T_c) needed to charge the system and the time to complete the transmission (T_{tx}), given by

$$\eta_d = \frac{d_m}{T_c + T_{tx}}. \tag{18}$$

To assess the source of loss for varying transmission power levels, the *power transfer efficiency* (PTE) of the wireless link can be measured as

$$\eta_{PTE} = \frac{P_{rx}}{P_{tx}} \times 100, \tag{19}$$

where P_{rx} is the received AC electrical power before the rectifier and P_{tx} is the transmitted AC electrical power. PTE will quantify the power loss due to the combined effect of the transducer electro-acoustic and acousto-electric conversion losses and the attenuation in water. Moreover, to evaluate the loss caused by the rectifier, we can measure the *rectifier efficiency* as the ratio between the DC rectified power and the received AC electrical power, given a certain load, which can be expressed as

$$\eta_{rect} = \frac{P_{dc}}{P_{rx}} \times 100. \tag{20}$$

Finally, we define the global *system efficiency* as the ratio between the DC rectified power and the transmitted AC electrical power, given by

$$\eta_{sys} = \frac{P_{dc}}{P_{tx}} \times 100. \tag{21}$$

Current System Limitations

Specifically, in our approach, since we use the same transducer for powering and data communication, the device cannot communicate during the charging phase. Even though, ultrasonic WPT proved to be more efficient than alternative WPT methods, the charging times are still a bottleneck in the system operations, therefore using a secondary storage and another transducer will allow the device to operate also during charging. Another limitation is represented by the use of focused transducers, therefore a certain grade of alignment is still required between the transmitter and the receiver. To enable a more flexible system, omnidirectional or partially directional transducers could be used. However, this becomes very challenging and inefficient because of power loss in different directions. An alternative solution to this problem could be a charger that uses an array of transducers with steerable beamforming capabilities and feedback from the nodes.

6 System Prototype

An illustration of the experimental testbed is depicted in Figure 10. The system is tested in a water tank. Our testing setup consists of a power transmitting station (left side of the tank) and a transceiver node prototype. The IoUT platform includes an energy management unit, a powering unit, and an underwater SEANet G1 sensor node based on the architectural model reported in Section 5. The printed circuit board (PCB) implementing the SEANet G1 node is showed in Figure 11 in more detail.

The charging station that transmits power to the submerged node is composed of three main elements: a

This article has been accepted for publication in a future issue of this journal, but has not been fully edited. Content may change prior to final publication. Citation information: DOI 10.1109/TMC.2020.3029679, IEEE Transactions on Mobile Computing

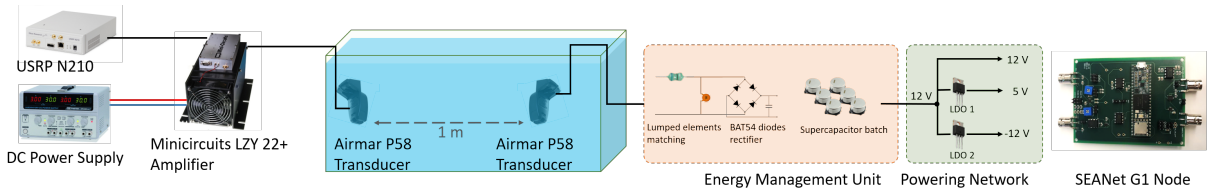

Fig. 10. Schematic illustration of the testbed used to demonstrate the ultrasonic WPT in water and powering of the SEANet G1 node.

Universal Software Radio Peripheral-based (USRP)-based software-defined underwater modem [38], [39], [40] (to generate the signals at ultrasound frequencies), a Mini-Circuits LZY-22+ high-power amplifier, and an Airmar P58 transducer. The USRP-based modem, incorporating a general purpose processor (GPP), leverages an open source software framework called GNU Radio for generating baseband samples. The generated baseband samples are then sent to a commercially available software-defined radio platform, USRP N210, through a Gigabit Ethernet (GigE) interface. The USRP N210, equipped with LFTX and LFRX daughterboards (supporting DC-30 MHz), enables the generation of waveforms in the frequency range (35 kHz to 65 kHz) of the selected transducer, Airmar P58. Specifically in this setup, the charging station is using 50 kHz sinusoidal signals for maximizing the transferred power, as Airmar P58 transducers have their highest electro-acoustic conversion efficiency, both for reception and transmission, at 50 kHz. The waveforms generated by the USRP are then amplified by the LZY-22+ high-power amplifier, which is powered by a DC power supply (GW Instek GPS-3303). Finally, the amplified waveforms are converted to ultrasonic waves by the Airmar P58 transducer.

The submerged IoUT node incorporates a matching network based on a passive lumped element circuit for limiting the signal leakage and reflections between the mode and the transducer to picoamperes for receiving the maximum input power. Moreover, the IoUT node leverages a rectifier that is based on a traditional full wave AC-to-DC converter realized with BAT54 diodes. As for the storage, the submerged IoUt node includes six 5.5 V off-the-shelf supercapacitors, of which four are 100 mF and two are 47 mF. During the charging phase the supercapacitors are all connected in parallel. The maximum equivalent voltage that can be reached across this configuration is still 5.5V (which is easier to reach after the attenuation in water) and the equivalent capacity seen from the rectifier is 494 mF. During the powering phase we change the supercapacitors configuration. Two sets of 100-100-47 mF series-connected supercapacitors are connected in parallel so that the total equivalent capacity is 48.45mF and the equivalent voltage across the new capacity configuration is 15 V, namely the sum of the voltages across each capacitor in one of the two series branch. 48.45 mF at 15 V gives enough energy ($\sim$ 5 J) to power up the communication unit, perform sensor readings for 800 ms and transmit one packet (one ZP-OFDM packet including eight ZP-OFDM symbols carrying 6144 bits of data). Finally, two LDOs are included in the powering unit to regulate the voltage supplied from the supercapacitors to the SEANet G1 components, providing different voltage levels to each device according to its specific powering requirement. As shown in Figure 3, a 12 V-to-5 V LDO provides a 5 V voltage to the Teensy from the supercapacitors, and a 12 V-to-$(-12$ V) LDO converts the voltage for the negative rail of the mixer. The power amplifier and the positive rail of the mixer can be powered directly from the +12 V energy buffer.

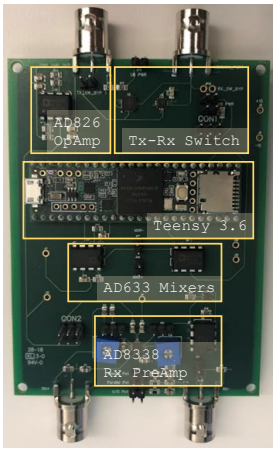

Fig. 11. PCB implementing a SEANet G1 node.

7 Experimental Results

In this Section, we present three sets of experiments to showcase the feasibility of the Ultrasonic WPT and the battery-less IoUT platforms. We first report on the transmission power of the proposed system. Then, we focus on measuring the efficiency of an ultrasonic wireless link as well as the proposed system's efficiency including rectifier efficiency. Finally, we concentrate on showcasing the overall charging efficiency and the actual amount of data that can be transmitted with the received power.

Transmission Power of the Proposed System

In this first set of experiments, we focus on measuring the transmission power of the charging station to assess the

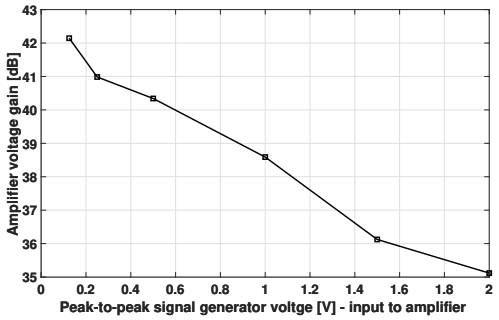

Fig. 12. Gain of the Micro-Circuits LZY-22+ amplifier for varying input peak-to-peak voltage.

This article has been accepted for publication in a future issue of this journal, but has not been fully edited. Content may change prior to final publication. Citation information: DOI 10.1109/TMC.2020.3029679, IEEE Transactions on Mobile Computing

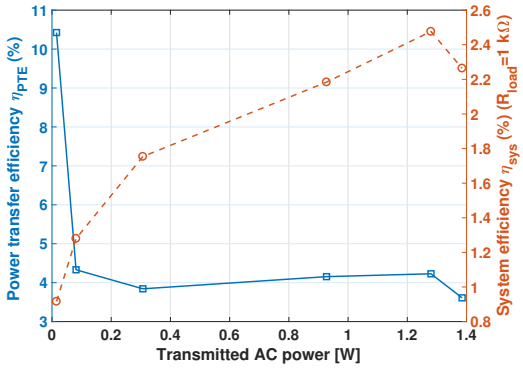

Fig. 13. Wireless link efficiency and system efficiency vs. transmitted electrical power.

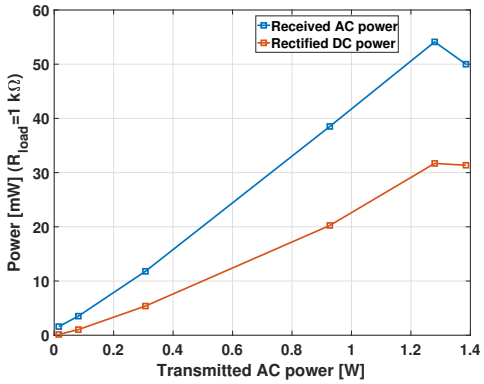

Fig. 15. AC received power and AC-to-DC rectified power at the receiver when the rectifier is connected to a $1\ \mathrm{k}\Omega$ resistive load for varying transmit power.

wireless power transmission capability of the current system. To that end, we measure the voltage gain of the Micro-Circuits LZY-22+ amplifier operating at the maximum DC supply voltage of $24\ \mathrm{V}$ for different values of the peak-to-peak input voltage of the waveforms coming from the USRP. Particularly, the peak-to-peak values of the generated sinusoidal waveforms (ranging from 0.15V to 2V) and their relative voltage amplification gains spanning from $42.3\ \mathrm{dB}$ to $35.2\ \mathrm{dB}$ are reported in Figure 12. The voltage gain decreases of $7\ \mathrm{dB}$ (2.24 times) when the input swipes from $0.125\ \mathrm{V}$ peak-to-peak to $2\ \mathrm{V}$ peak-to-peak. Hence, it would make sense to operate at the maximum USRP output of $2\ \mathrm{V}$ which gives the highest transmit voltage of $112.4\,\mathrm{V}$ peak-to-peak. However, the *power transfer efficiency (PTE)* also needs to be taken into account. In fact, the maximum PTE, as showed in Figure 13, is reached when the input power is $1.28\ \mathrm{W}$. This power is obtained when the USRP voltage is set to $1.5\,\mathrm{V}$ peak-to-peak which is later amplified up to $96\,\mathrm{V}$ peak-to-peak. Please note that, a Tektronix - CT6 current probe is used for measuring all the electrical power levels.

Efficiency of an Ultrasonic Link and the Proposed System

We used the experimental testbed illustrated in Figure 10 to measure and characterize the efficiency of an ultrasonic wireless link, specifically at a $1\ \mathrm{m}$ range. We first measure the *power transfer efficiency (PTE)* of the $1\,\mathrm{m}$-link, as shown in Figure 13. The *PTE* is observed to be varying between 10% and 4% for transmission power levels lower than $0.1\ \mathrm{W}$, while it is almost flat around 4% for transmission power levels larger than $0.1\ \mathrm{W}$.

To further analyze the observed *PTE*, we focus on quantifying the link loss including the loss due to non-ideal electric-acoustic and acoustic-electric conversions of the transducers, as well as measuring the loss due to the rectifier by connecting the output of the rectifier to a $1\ \mathrm{k}\Omega$ load. Figure 14 showcases the rectifier efficiency (η_{rect}) for varying received AC electrical power levels. The results prove that with at least $30\ \mathrm{mW}$ of AC electrical power, the designed rectifier can work with an efficiency of more than 50%. Furthermore, we measured the efficiency of the whole system (η_{sys}) as illustrated in Figure 13. As expected, the combined effect of η_{pte} and η_{rect} leads to a system efficiency of 2% for a transmission power level of $1\ \mathrm{W}$.

In Figure 15, we report the AC received electrical power and its relative rectifier output (rectified DC power). As it can be observed, the rectifier efficiency increases as the transmit power increases. For example, for a transmit power of $0.3\,\mathrm{W}$, the system receives an AC power of approximately $12\,\mathrm{mW}$ and accordingly obtains a DC power of $6\,\mathrm{mW}$ which corresponds to an approximate rectifier efficiency of 50%. On other hand, for a higher transmit power level such as $1.28\ \mathrm{W}$, the system receives an AC power level of $53.5\ \mathrm{mW}$ which then converted into a DC power level of $32.5\ \mathrm{mW}$ corresponding to an approximate rectifier efficiency of a little over 60%.

Another important observation that can be obtained from the Figure 15 is about the transmission power levels above $1.28\ \mathrm{W}$. As it can be seen, even if the transmission power levels increase, the received AC power levels and accordingly η_{pte} and η_{sys} decrease or stay the same as shown in Figure 15. We believe that, there can be two possible explanations to this phenomena. First, the Airmar P58 transducer might have reached its peak source level ($205\ \mathrm{dB}$) and it starts saturating. Second and more likely reason is the cavitation. Cavitation is a phenomenon that appears in rapid pressure changes of pressure that lead to formation of small vapor-filled cavities or voids. So when transducers are driven with higher power levels, especially under lower pressure conditions (at lower depths), they generally get those air voids around them which weakens their ultrasonic pressure levels. Given the nature of our testbed setup, which has the transducers deployed only at a depth of few meters, occurrence of cavitation is very likely at very higher power levels (i.e. above $1.28\ \mathrm{W}$).

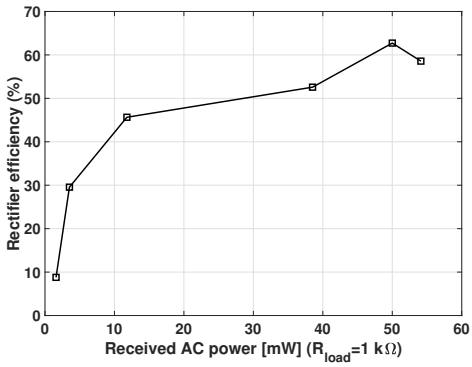

Fig. 14. Rectifier efficiency η_{rect} vs. the received AC power with a $1\ \mathrm{k}\Omega$ load.

This article has been accepted for publication in a future issue of this journal, but has not been fully edited. Content may change prior to final publication. Citation information: DOI 10.1109/TMC.2020.3029679, IEEE Transactions on Mobile Computing

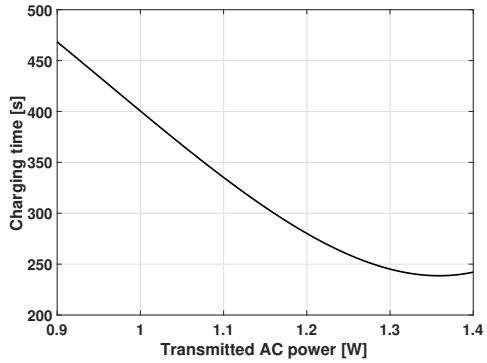

Fig. 16. Charging time (seconds) as function of the transmitted AC power (W).

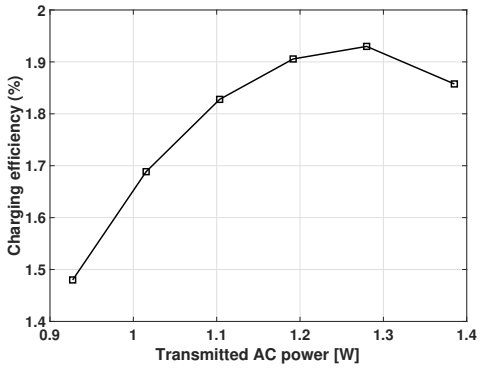

Fig. 17. System charging efficiency for different values of the transmitted electrical power.

Charging Efficiency and Effective Data Rate

In this set of experiments, we focus on observing the charging efficiency and the actual amount of data that can be transmitted with the received power. To this end, as explained in Section 6, we charged a set of supercapacitors and we recorded the time to charge the storage with different amounts of transmitted power. Figure 16 reports the observed charging time as a function of the transmitted AC power. As it is expected, charging time becomes shorter for higher transmitted AC power levels.

Experimental results for the charging efficiency (η_c) are shown in Figure 17. Since E_s is constant, and we observe that the charging times become shorter with an increase in transmitted power, the decrease of η_c is due to the decrease of the PTE (η_{PTE}) around 1.3 W (compare Figure 13 with Figure 17).

Finally, we measure the effective data rate. Once the supercapacitors are charged up to 5 V, their configuration is changed to provide an initial voltage of 15 V to power the IoUT system. Figure 18 shows that the effective data rate, as defined in (18), increases relative to the transmitted power. This can be explained by the fact that higher transmitted power levels reduce the charging time which will eventually lead to higher effective data rates.

8 Conclusions

Powering of systems deployed in deep waters remains one of the core challenges toward the long-term deployment of untethered underwater systems. In this article, we

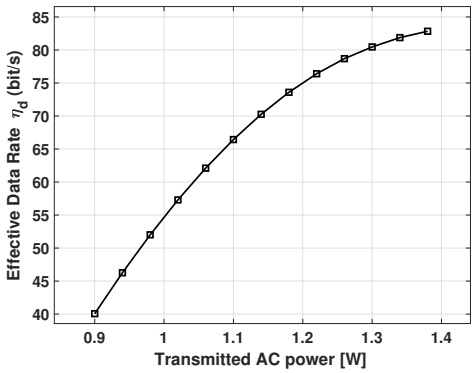

Fig. 18. System effective data rate η_d for different values of the transmitted electrical power.

presented the first ultrasonically rechargeable underwater sensor node. The system is batteryless and powered by supercapacitors whose charge can be restored by means of ultrasonic WPT realized over distances longer than current inductive and magnetic technologies. We reported on the architectural model of an underwater platform capable of extracting electrical power from ultrasonic waves and using it to power an ultrasonic communication system. We realized a prototype based on the proposed architecture. Experimental results proved that the collected energy is sufficient to perform a sensing operation and power an underwater acoustic modem for communications.

References

[1] R. Guida, E. Demirors, N. Dave, J. Rodowicz, and T. Melodia, "Acoustically Powered Battery-less Internet of Underwater Things Platform," in *Proc. of IEEE Underwater Communications Conf. And Workshop (UComms)*, Lerici, Italy, August 2018.

[2] I. F. Akyildiz, D. Pompili, and T. Melodia, "Underwater acoustic sensor networks: research challenges," *Ad hoc networks*, vol. 3, no. 3, pp. 257–279, 2005.

[3] J. Heidemann, M. Stojanovic, and M. Zorzi, "Underwater sensor networks: applications, advances and challenges," *Philosophical Transactions of the Royal Society of London A: Mathematical, Physical and Engineering Sciences*, vol. 370, no. 1958, pp. 158–175, 2012.

[4] T. Melodia, H. Kulhandjian, L. Kuo, and E. Demirors, "Advances in Underwater Acoustic Networking," in *Mobile Ad Hoc Networking: Cutting Edge Directions*, second edition ed., S. Basagni, M. Conti, S. Giordano, and I. Stojmenovic, Eds. Inc., Hoboken, NJ: John Wiley and Sons, 2013, pp. 804–852.

[5] A. Davis and H. Chang, "Underwater wireless sensor networks," in *Proc. of Oceans*. IEEE, 2012, pp. 1–5.

[6] L. Pessoa, M. Pereira, H. Santos, and H. Salgado, "Simulation and experimental evaluation of a resonant magnetic wireless power transfer system for seawater operation," in *Proc. of Oceans*. Shanghai, China: IEEE, 2016, pp. 1–5.

[7] B. S. Srujana, P. Mathews, V. Harigovindan *et al.*, "Multi-source energy harvesting system for underwater wireless sensor networks," *Procedia Computer Science*, vol. 46, pp. 1041–1048, 2015.

[8] A. M. Bradley, M. D. Feezor, H. Singh, and F. Y. Sorrell, "Power Systems for Autonomous Underwater Vehicles," *IEEE Journal of oceanic Engineering*, vol. 26, no. 4, pp. 526–538, 2001.

[9] C. Detweiller, I. Vasilescu, and D. Rus, "An underwater sensor network with dual communications, sensing, and mobility," in *Oceans 2007*. IEEE, 2007, pp. 1–6.

[10] A. Dewan, S. U. Ay, M. N. Karim, and H. Beyenal, "Alternative Power Sources for Remote Sensors: A Review," *Journal of power sources*, vol. 245, pp. 129–143, 2014.

[11] S. Basagni, V. Di Valerio, P. Gjanci, and C. Petrioli, "Harnessing HyDRO: Harvesting-aware Data ROuting for Underwater Wireless Sensor Networks," in *Proc. of ACM Intl. Symposium on Mobile Ad Hoc Networking and Computing*. ACM, 2018, pp. 271–279.

[12] M. C. Domingo, "An overview of the internet of underwater things," *Journal of Network and Computer Applications*, vol. 35, no. 6, pp. 1879–1890, 2012.

[13] Y. Cha, H. Kim, and M. Porfiri, "Energy harvesting from underwater base excitation of a piezoelectric composite beam," *Smart materials and Structures*, vol. 22, no. 11, p. 115026, 2013.

[14] G. W. Taylor, J. R. Burns, S. Kammann, W. B. Powers, and T. R. Welsh, "The Energy Harvesting Eel: a Small Subsurface Ocean/River Power Generator," *IEEE journal of oceanic engineering*, vol. 26, no. 4, pp. 539–547, 2001.

[15] F. K. Shaikh and S. Zeadally, "Energy harvesting in wireless sensor networks: A comprehensive review," *Renewable and Sustainable Energy Reviews*, vol. 55, pp. 1041–1054, 2016.

[16] C. R. Rodrigues, C. A. Alves, J. Puga, A. M. Pereira, and J. O. Ventura, "Triboelectric driven turbine to generate electricity from the motion of water," *Nano energy*, vol. 30, pp. 379–386, 2016.

[17] Y. Su, X. Wen, G. Zhu, J. Yang, J. Chen, P. Bai, Z. Wu, Y. Jiang, and Z. L. Wang, "Hybrid Triboelectric Nanogenerator for Harvesting Water Wave Energy and as a Self-Powered Distress Signal Emitter," *Nano Energy*, vol. 9, pp. 186–195, 2014.

[18] T. Ewing, P. T. Ha, and H. Beyenal, "Evaluation of long-term performance of sediment microbial fuel cells and the role of natural resources," *Applied Energy*, vol. 192, pp. 490–497, 2017.

[19] A. Capitaine, G. Pillonnet, T. Chailloux, O. Ondel, and B. Allard, "10 μW Converter for Energy Harvesting from Sedimentary Microbial Fuel Cells," *IEEE Intl. Midwest Symposium on Circuits and Systems (MWSCAS)*, pp. 337–340, 2017.

[20] R. Umaz, C. Garrett, F. Qian, B. Li, and L. Wang, "A power management system for multianode benthic microbial fuel cells," *IEEE Transactions on power electronics*, vol. 32, no. 5, 2017.

[21] C. Donovan, A. Dewan, H. Peng, D. Heo, and H. Beyenal, "Power management system for a 2.5 w remote sensor powered by a sediment microbial fuel cell," *Journal of Power Sources*, vol. 196, no. 3, pp. 1171–1177, 2011.

[22] N. B. Carvalho, A. Georgiadis, A. Costanzo, N. Stevens, J. Kracek, L. Pessoa, L. Roselli, F. Dualibe, D. Schreurs, S. Mutlu *et al.*, "Europe and the future for WPT," *IEEE Microwave Magazine*, vol. 18, no. 4, pp. 56–87, 2017.

[23] M. Kesler and C. McCarthy, "Highly resonant wireless power transfer in subsea applications," *WiTricity white paper*, 2013, [Online]. Available: https://tinyurl.com/s5vzhbx.

[24] N. W. Bergmann, J. Juergens, L. Hou, Y. Wang, and J. Trevathan, "Wireless underwater power and data transfer," in *Proc. of IEEE Workshop on Local Computer Networks (LCN)*, 2013, pp. 104–107.

[25] Z. Cheng, Y. Lei, K. Song, and C. Zhu, "Design and loss analysis of loosely coupled transformer for an underwater high-power inductive power transfer system," *IEEE Transactions on Magnetics*, vol. 51, no. 7, pp. 1–10, 2015.

[26] K. Shizuno, S. Yoshida, M. Tanomura, and Y. Hama, "Long Distance High Efficient Underwater Wireless Charging System Using Dielectric-assist Antenna," in *2014 Oceans-St. John's*. IEEE, 2014.

[27] Z.-S. Li, D.-J. Li, L. Lin, and Y. Chen, "Design considerations for electromagnetic couplers in contactless power transmission systems for deep-sea applications," *Journal of Zhejiang University SCIENCE C*, vol. 11, no. 10, pp. 824–834, 2010.

[28] E. Demirors, J. Shi, R. Guida, and T. Melodia, "Seanet G2: toward a high-data-rate software-defined underwater acoustic networking platform," in *Proc. of ACM Intl. Conf. on Underwater Networks & Systems (WUWNet)*, Shanghai, China, 2016, p. 12.

[29] A. Bereketli and S. Bilgen, "Remotely powered underwater acoustic sensor networks," *IEEE Sensors Journal*, vol. 12, no. 12, 2012.

[30] EEWorld Online, "Navy's Underwater Wireless Charging Station Can Improve Remote UUV Mission Performance," [Online]. Available: https://tinyurl.com/y8e786nu.

[31] E. Demirors, B. G. Shankar, G. E. Santagati, and T. Melodia, "SEANet: a software-defined acoustic networking framework for reconfigurable underwater networking," in *Proc. of ACM Intl. Conf. on Underwater Networks & Systems (WUWNet)*, 2015, p. 11.

[32] A. I. Al-Shamma'a, A. Shaw, and S. Saman, "Propagation of Electromagnetic Waves at MHz Frequencies Through Seawater," *IEEE Transactions on Antennas and Propagation*, vol. 52, no. 11, 2004.

[33] S. Jiang and S. Georgakopoulos, "Electromagnetic wave propagation into fresh water," *Journal of Electromagnetic Analysis and Applications*, vol. 3, no. 07, p. 261, 2011.

[34] E. A. Karagianni, "Electromagnetic waves under sea: bow-tie antennas design for wi-fi underwater communications," *Progress In Electromagnetics Research*, vol. 41, pp. 189–198, 2015.

[35] M. C. Domingo, "Magnetic induction for underwater wireless communication networks," *IEEE Transactions on Antennas and Propagation*, vol. 60, no. 6, pp. 2929–2939, 2012.

[36] A. Zoksimovski, D. Sexton, M. Stojanovic, and C. Rappaport, "Underwater electromagnetic communications using conduction–channel characterization," *Ad Hoc Networks*, vol. 34, 2015.

[37] M. A. Ainslie and J. G. McColm, "A simplified formula for viscous and chemical absorption in sea water," *The Journal of the Acoustical Society of America*, vol. 103, no. 3, pp. 1671–1672, 1998.

[38] E. Demirors, G. Sklivanitis, G.E. Santagati, T. Melodia and S. N. Batalama, "Design of A Software-defined Underwater Acoustic Modem with Real-time Physical Layer Adaptation Capabilities," in *Proc. of ACM Intl. Conf. on Underwater Networks & Systems (WUWNet)*, Rome, Italy, November 2014.

[39] E. Demirors, G. Sklivanitis, T. Melodia, S. N. Batalama, and D. A. Pados, "Software-defined underwater acoustic networks: Toward a high-rate real-time reconfigurable modem," *IEEE Communications Magazine*, vol. 53, no. 11, pp. 64–71, November 2015.

[40] E. Demirors, G. Sklivanitis, G. E. Santagati, T. Melodia, and S. N. Batalama, "A high-rate software-defined underwater acoustic modem with real-time adaptation capabilities," *IEEE Access*, vol. 99, pp. 1–1, 2018.

Raffaele Guida (S'15) received the B.S. and M.S. degrees in telecommunication engineering from University of Sannio, Benevento, Italy, in 2009 and Sapienza University of Rome, Rome, Italy, in 2013, respectively. He is currently a Ph.D. candidate with the Department of Electrical and Computer Engineering, Northeastern University, Boston, MA, USA. He is also with Wireless Networks and Embedded Systems Laboratory, Northeastern University, under the guidance of Prof. Tommaso Melodia. His current research interests are in intra-body wireless networks, ultrasonic energy transfer, and implantable medical devices.

Emrecan Demirors (S'11, M'17) received the Ph.D. degree in Electrical and Computer Engineering from the Northeastern University, Boston, MA, USA, in 2017. He is a Research Assistant Professor with the Department of Electrical and Computer Engineering at Northeastern University. His research interests include underwater communications, networking, and systems; Internet of Medical Things; 5G and IoT. Dr. Demirors is the recipient of the Best Paper Awards of ACM WUWNet 2015 and 2016; IEEE WoWMoM 2019; IEEE ACM WiNTECH 2019. He is an Associate Editor for the IEEE Access.

Neil Dave Received his B.S in electrical engineering from Northeastern University in Boston, MA, USA in 2016. He is currently a M.S candidate with the department of Electrical and Computer Engineering, Northeastern University, Boston, MA, USA and works in the Wireless Networks and Embedded Systems Laboratory under the guidance of advisor Pr. Tommaso Melodia. His primary research interests are in ultrasonic intra-body sensor networks, biomedical devices and underwater communications.

Tommaso Melodia (M'07, SM'16, F'18) received the Ph.D. degree in Electrical and Computer Engineering from the Georgia Institute of Technology in 2007. He is the William Lincoln Smith Professor with the Department of Electrical and Computer Engineering of Northeastern University. He is the Director of Research for the PAWR Project Office, a public-private partnership that is developing four city-scale platforms for advanced wireless research in the United States. Prof. Melodia's research focuses on modeling, optimization, and experimental evaluation of wireless networked systems, with applications to 5G Networks and Internet of Things, software-defined networking, and body area networks. Prof. Melodia is an Associate Editor for the IEEE Transactions on Mobile Computing, the IEEE Transactions on Biological, Molecular, and Multi-Scale Communications, Computer Networks, and Smart Health. Prof. Melodia's research is supported mostly by U.S. federal agencies including the National Science Foundation, the Air Force Research Laboratory, the Office of Naval Research, and the Army Research Laboratory. He is a Fellow of the IEEE and a Senior Member of the ACM.